



Universidad Autónoma
de Madrid

Biblos-e Archivo
Repositorio Institucional UAM

Repositorio Institucional de la Universidad Autónoma de Madrid
<https://repositorio.uam.es>

Esta es la **versión de autor** del artículo publicado en:
This is an **author produced version** of a paper published in:

Chemosphere 281 (2021): 130885

DOI: <https://doi.org/10.1016/j.chemosphere.2021.130885>

Copyright: © 2021 Elsevier Ltd. This manuscript version is made available under the CC-BY-NC-ND 4.0 licence <http://creativecommons.org/licenses/by-nc-nd/4.0/>

El acceso a la versión del editor puede requerir la suscripción del recurso
Access to the published version may require subscription

Continuous aqueous phase reforming of a synthetic brewery wastewater with Pt/C and PtRe/C catalysts for biohydrogen production

A. S. Oliveira¹, T. Cordero-Lanzac², J. A. Baeza¹, L. Calvo^{1*}, F. Heras¹, J. J. Rodriguez¹,
M. A. Gilarranz¹

¹Department of Chemical Engineering, Universidad Autónoma de Madrid, 28049
Madrid, Spain

²Department of Chemical Engineering, University of the Basque Country, 48080, Bilbao,
Spain

*corresponding author e-mail: luisa.calvo@uam.es Tel: +34 914 97 87 74

Abstract

This work investigates H₂ production through aqueous phase reforming (APR) of synthetic brewery wastewater in a continuous fixed bed reactor with Pt and PtRe (3 wt. %) catalysts supported on activated carbon. The influence of weight hourly space velocity (WHSV) and superficial Ar gas flow velocity (V_{Ar}) was assessed for the sake of optimisation, while reaction temperature and pressure were maintained at 225 °C and 28 bar, respectively. H₂ production was found to be higher using the PtRe catalyst at the lowest WHSV (0.03 h⁻¹) and highest V_{Ar} (0.8 cm s⁻¹). The comparison of the maximum H₂ production obtained in this work (27.9 μmol min⁻¹) with other treatment processes shows the potential of the application of APR process for H₂ production from brewery wastewater. Despite the different reaction conditions tested, the catalysts showed deactivation with time on stream, which was related to the formation of solid deposits on the surface of the catalysts. Therefore, future research should be related to the development of more stable catalysts, strategies that avoid deactivation by coking and regeneration processes.

Keywords: biohydrogen, aqueous phase reforming, brewery wastewater, deactivation

1. Introduction

Aqueous phase reforming (APR) is a catalytic process for H₂ and alkanes production from biomass derived compounds that is carried out under relative mild reaction conditions (200 – 250 °C and 15 – 50 bar) over metal catalysts (Cortright et al., 2002). This process shows some advantages when compared to other H₂ production process such as steam reforming. For instance, the reaction conditions reduce energy consumption, facilitate the purification of produced gas, minimize undesired decomposition reactions of starting compounds, and favour the water-gas shift (WGS) reaction, which allows producing H₂ with negligible CO content (Cortright et al., 2002; Davda et al., 2005). Furthermore, APR is energy efficient and the total cost of H₂ production can be lower than that of autoreforming and steam reforming (Khodabandehloo et al., 2020; Martín and Grossmann, 2014). On the other hand, the theoretical maximum H₂ yields in the APR process are 50% higher than in biological processes such as fermentation, i.e. 6 and 4 mol H₂ per mol glucose, respectively.

The main reactions involved in H₂ production through APR of oxygenated hydrocarbons with C:O ratio equal to 1:1 can be represented by Equations (1) and (2), the latest corresponding to WGS reaction.



Regarding the catalysts, Pt monometallic catalysts are widely used in APR due to the higher H₂ selectivity obtained (Davda et al., 2003), whereas bimetallic catalysts have been found to achieve better activity than monometallic ones (Godina et al., 2018a; Huber et al., 2006). Particularly interesting results have been obtained with PtRe catalysts, in comparison to other Pt-based bimetallic ones such as PtNi, PtRu and PtCo (Godina et al.,

2018a). Regarding the substrates, a variety of model compounds such as ethylene glycol, glycerol or sorbitol have been used in APR, mainly for H₂ production, showing promising results in terms of conversion and H₂ selectivity and yield (Cortright et al., 2002; Kirilin et al., 2012; Shabaker et al., 2004). On the other hand, although APR may be considered more suitable for processing dilute side streams than gasification, there are few studies using this type of streams as feedstocks (Aho et al., 2020; Pipitone et al., 2020). In this sense, biomass-derived wastewaters, such as that from brewery and fruit juice production, has been proposed as feedstock for treatment through APR (Oliveira et al., 2019; Saenz de Miera et al., 2020). This new application integrates wastewater treatment and valorisation of waste effluents, combining organic matter removal and H₂ production. In addition, it is interesting to evaluate the processability of waste effluents, since technological studies have reported that the cost of the substrate is an important drawback to APR process feasibility, representing almost 92% of the total cost of H₂ produced (Sladkovskiy et al., 2018).

Previous studies on the use of APR for the treatment and valorisation of wastewater have focussed mainly on the influence of catalysts properties and the effect of variables such as temperature, basicity and organic load of the wastewater in batch reactors (Oliveira et al., 2018, 2020a, 2019). However, these reactors are not suitable for large scale operation, especially when diluted feedstocks such as some wastewaters, are processed, and make difficult to achieve conclusive results on catalyst stability. In addition to this, the use of continuous reactors facilitates the evaluation of other operating variables such as contact time of substrate over the catalyst and H₂ stripping by the carrier gas flow, which can significantly affect the performance of the catalysts in APR. Kim et al. (2012) studied the APR ethylene glycol with a PtRe/C catalyst at weight hourly space velocity (WHSV) values varying between 1 – 6 h⁻¹. They reported that H₂ yield and carbon conversion to

gas were higher at low WHSV (1 h^{-1}), whereas the selectivity to H_2 and alkanes was not significantly affected. In contrast, Duarte et al. (2017) reported that in the APR of xylitol with $\text{Pt}/\text{Al}_2\text{O}_3$ catalyst, H_2 selectivity increased and both H_2 yield and xylitol conversion to gas diminished when WHSV increased from 0.4 to 2.4 h^{-1} , which was attributed to a lower H_2 consumption in side reactions due to shorter contact time. On the other hand, Kirilin et al. (2012) found that in the APR of xylitol and sorbitol using $\text{Pt}/\text{Al}_2\text{O}_3$ catalyst, the H_2 selectivity peaked in the range of WHSV from 0.6 to 3.9 h^{-1} , while xylitol/sorbitol conversion decreased with increasing WHSV. The maximum in H_2 selectivity resulted from the combination of higher xylitol/sorbitol conversion and higher H_2 consumption in side reactions at long contact time.

Regarding the effect of the carrier gas flow, the use of an inert gas as a stripping agent promotes H_2 mass transfer and decreases the partial pressure of H_2 due to removal from the catalyst surface, enhancing reforming rate and limiting H_2 consumption in side reactions (Neira D'Angelo et al., 2013b, 2013a). Neira D'Angelo et al. (2014) reported that the use of a carrier gas was essential to obtain high activity and selectivity. Thus, increasing the ratio of carrier gas from 0 to $2 \text{ m}^3 \text{ N}_2$ per m^3 of liquid, increased the conversion and the H_2 selectivity by a factor of 2.4 and 5.2, respectively, in the APR of sorbitol. However, an excessive gas flow can be detrimental due to poorer wetting and channelling, which results in worse gas-liquid-solid contact (Neira D'Angelo et al., 2013a).

Accordingly, the aim of the current work is to evaluate the effect of WHSV and superficial velocity of the carrier gas (V_{Ar}) to find the reaction conditions that favours H_2 production by APR of brewery wastewater in continuous reactors with Pt and PtRe catalysts supported on activated carbon.

2. Experimental

2.1. Materials

The commercial activated carbon used as catalyst support (MER) was supplied by Merck. Hexachloroplatinic acid solution (8 wt.% in H₂O), perrhenic acid solution (75 – 80 wt.% in H₂O), maltose (D-(+)-Maltose monohydrate, \geq 99%), malt extract, wheat peptone, yeast extract, ammonium sulphate (\geq 99%) and KOH (\geq 99%) were purchased from Sigma-Aldrich. Ethanol (\geq 99.5%) was supplied by Panreac AppliChem.

2.2. Preparation and characterization of supports and catalysts

Pt/MER (3 wt.%) catalyst was prepared by incipient wetness impregnation and PtRe/MER (3 wt.%, metal ratio 1:2) catalyst was prepared by sequential incipient wetness impregnation, both using MER as support. After impregnation, the catalysts were oven-dried overnight at 60 °C, then Pt/MER was calcined at 200 °C and PtRe/MER was calcined at 250 °C, in both cases for 2 h at maximum temperature and using a heating rate of 10 °C per min, and then they were reduced at 300 °C for 2 h at maximum temperature using a heating rate of 10 °C per min under H₂ flow (25 N mL per min and g of catalyst). Reduction temperatures were selected according to previous thermal programmed reduction results (Ciftci et al., 2014a).

The support and catalysts were characterized by N₂ adsorption-desorption at 77 K (TriStar II, Micromeritics), pH slurry measurements and scanning transmission electron microscopy (STEM, JEOL - 3000F). The used catalysts were oven-dried overnight at 60 °C before characterization. Before N₂ adsorption-desorption analysis, the catalysts were degassed under vacuum at 150 °C for 4 h. The pH slurry was determined by measuring the pH of an aqueous suspension of the support or catalyst, using 1 g of solid in 10 mL of distilled water. The metal nanoparticles (NPs) size was assessed from digital STEM

images using "ImageJ 1.51k" software. More than 200 NPs per catalyst were used to calculate the mean size and size distribution.

Used catalysts were also characterized by elemental analysis (LECO CHNS-932) and thermogravimetric analysis (TGA Q500, TA Instruments and TG-TPD/TPO). The CHNS-O composition of the catalysts was calculated by means of elemental analysis (LECO CHNS-932), being O concentration calculated by difference. In the temperature-programmed desorption (TG-TPD) analysis, the samples were first subjected to a continuous flow of N₂ (50 N mL min⁻¹) at 450 °C for 30 min (heating rate of 10 °C per min) and then cooled to room temperature. The flow was then shifted to air and a temperature-programmed oxidation (TG-TPO) was performed at 550 °C during 2 h (heating rate of 5 °C per min).

2.3. Preparation and characterization of synthetic brewery wastewater

Synthetic brewery wastewater (SBW) was prepared according to literature (Habte Lemji and Eckstädt, 2013) and previous batch APR works (Oliveira et al., 2020a, 2019). KOH was added to the wastewater to adjust the pH value to 10, since real brewery wastewaters are usually basic due to the use of cleaning-in-place processes, frequently employed in food and beverages industries. The SBW was characterized by total organic carbon (TOC) analysis using a TOC-VCSH Shimadzu analyser and by chemical oxygen demand (COD) analysis using a standard method (ASTM D1252). The liquid samples of initial SBW were analysed in triplicate and TOC and COD values of 1968 ± 111 mg L⁻¹ and 6229 ± 341 mg L⁻¹ were obtained, respectively.

2.4. Aqueous phase reforming experiments

The APR experiments were carried out at 225 °C and 28 bar with 1 g of catalyst during 24 h time on stream (TOS), in a continuous vertical fixed bed reactor equipped with

temperature and pressure controllers. The reactor was heated externally, and the reaction temperature was monitored using a thermocouple placed inside the stainless steel reactor tube (300 x 10 mm i.d) above the catalyst. SBW was fed from the top of the reactor with a HPLC pump. WHSV was adjusted to 0.03, 0.12 and 0.48 h⁻¹, based on the C content of the influent (i.e. g of C per h and per g of catalyst), by feeding the wastewater at 0.25, 1 and 4 mL min⁻¹, respectively. High purity Ar (99.99%) was used to purge the reaction system and as carrier gas throughout the reaction. The effect of Ar gas flow was evaluated using 5, 20 and 40 N mL min⁻¹ flow rates, which are equivalent to V_{Ar} of 0.1, 0.4 and 0.8 cm s⁻¹, respectively. The gas stream exiting the reactor was analysed online by a gas chromatograph (GC/FID/TCD, 7820A, Agilent) equipped with two packed columns and a molecular sieve. The gas analysis included H₂, CO, CO₂, CH₄, C₂H₆ and C₃H₈ (error ± 5%). The liquid effluent was characterized in duplicate by TOC and COD measurements. TOC and COD removal (%) were determined as the difference between the initial and final TOC or COD value divided by the initial TOC or COD value (mg L⁻¹). Carbon conversion to gas (CC gas (%)) was calculated as the C content (g) in the gaseous products divided by the initial C content (g) in the brewery wastewater.

3. Results and discussion

3.1. Support and catalysts characterization

MER support yielded a BET surface area (S_{BET}) of 930 m² g⁻¹ and micropore and mesopore volumes of 0.38 and 0.15 cm³ g⁻¹, respectively (Table S1). The catalysts showed lower values of S_{BET} than the support due to metal loading, the difference being more pronounced in the case of PtRe/MER (800 m² g⁻¹). This last yielded also significantly lower pH slurry (5.8) than Pt/MER (8.5). Surface acidity of PtRe/C catalysts has been

attributed in literature to ReOx species (Chia et al., 2011) and Pt–O–Re structure (Zhang et al., 2012).

Pt/MER showed larger mean NPs size (4.6 nm) than PtRe/MER (3.6 nm) (Figure S1). In addition, it is important to mention that Pt/MER catalyst showed in some STEM images higher agglomeration of NPs (Figure S2), which were not considered in the histograms.

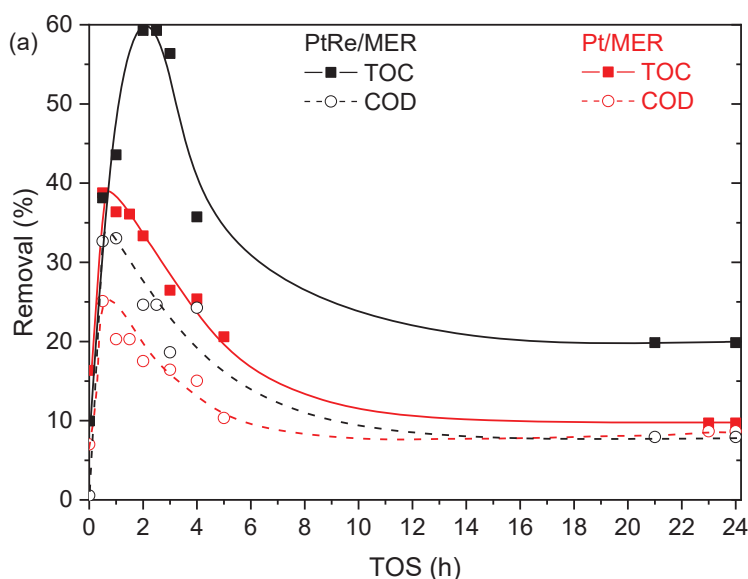
3.2. Catalysts performance

3.2.1. Comparison of Pt and PtRe catalysts

Pt/MER and PtRe/MER catalysts were compared at WHSV of 0.12 h⁻¹. The experiments were performed at V_{Ar} of 0.4 cm s⁻¹. Figure 1 (a) shows TOC and COD removal and (b) CC gas upon TOS. PtRe/MER catalyst showed higher TOC and COD removal than Pt/MER, indicating an enhanced activity due to the inclusion of Re. This can be ascribed to synergistic and/or promoting effects resulting from the combination of both metals, since monometallic Re catalysts have shown in general much lower activity than monometallic Pt ones in APR (Ciftci et al., 2014a). TOC and COD removal peaked at TOS values between 1 – 3 h for both Pt/MER and PtRe/MER catalysts. Around 1 h on stream was needed by Pt/MER catalyst to reach the maximum TOC removal, while PtRe/MER needed about 2 h, which may also indicate induction time due to acclimation of the catalysts. Some authors have interpreted this induction-like time as a stabilization stage where the metallic phase evolves to a more active structure (Godina et al., 2018b). After a relatively short time yielding maximum TOC and COD removal, the catalysts performance decreased evidencing significant deactivation.

For both Pt/MER and PtRe/MER catalysts, TOC was removed in a larger extent than COD, indicating that the O/C ratio in the remaining organic matter increased respect to the original constituents of the wastewater. The higher ratio between COD and TOC

removal for Pt/MER catalyst (e.g. 0.65 vs 0.42 for PtRe/MER at peak activity) may indicate different degradation routes depending on the active phases. Deactivation also provoked some changes in the degradation routes since the COD to TOC removal ratio increased to 0.89 for Pt/MER and decreased to 0.40 for PtRe/MER at long TOS values. Regarding CC gas, PtRe/MER yielded significantly higher value than Pt/MER (Figure 1 (b)). The peak values occurred at low TOS for both catalysts, consistently with the TOC and COD removal patterns, while the rapid sharp decrease confirms fast deactivation of both catalysts. Moreover, a large unbalance between the carbon removed from the liquid phase and the carbon in the gas produced was observed, especially in the first hours on stream where the carbon balance closure ranged from 41 to 74%, being the lowest values obtained for PtRe/MER. On the contrary, for longer time on stream the carbon balance closures were higher than 80%. This lack of carbon balance can be ascribed to the formation of carbonaceous solid upon hydrothermal carbonization (HTC) and deposition of condensation species, which can also contribute to catalysts deactivation.



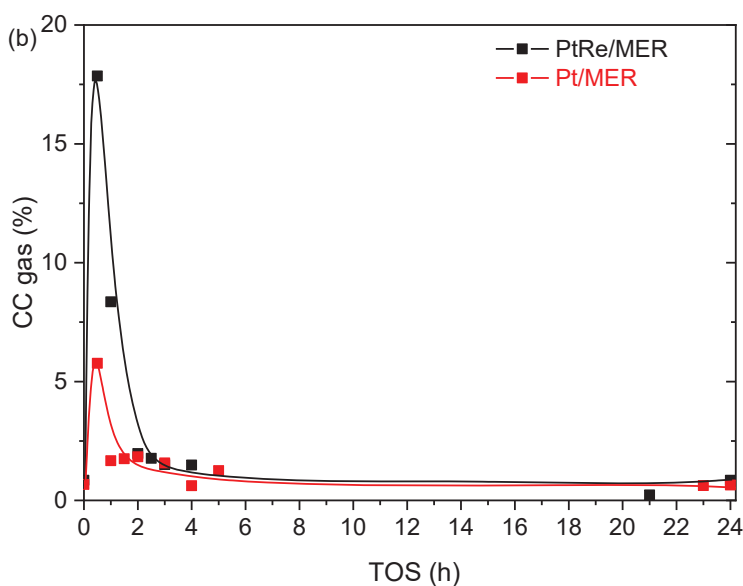


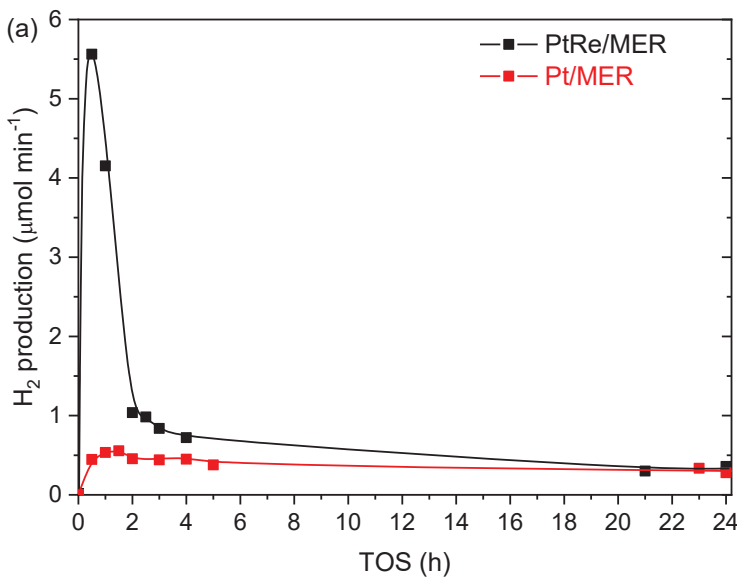
Figure 1. (a) TOC and COD removal and (b) CC gas upon time on stream in the APR of SBW with Pt/MER and PtRe/MER catalysts (225 °C, 28 bar, WHSV = 0.12 h⁻¹ and V_{Ar} = 0.4 cm s⁻¹)

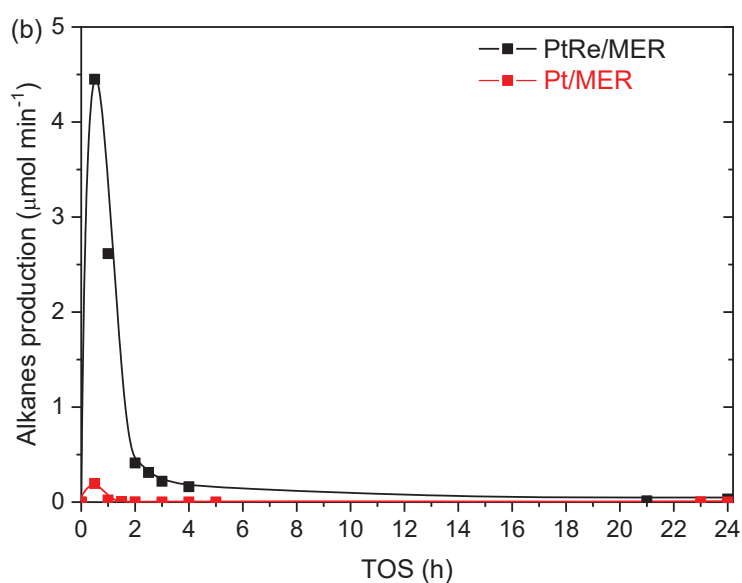
Figure 2 shows the evolution of H₂, total alkanes and CO₂ production upon TOS. CO was not detected along the experiments, indicating good conditions for water-gas shift (WGS) reaction. At low TOS values, PtRe/MER catalyst showed a higher activity than Pt/MER one for H₂ production. A maximum H₂ production of 5.6 μmol min⁻¹ (corresponding to 0.8 mmol H₂ g COD_{initial}⁻¹) and alkanes production of 4.4 μmol min⁻¹ (89.3% CH₄) were observed during the first hour on stream with PtRe/MER. Pt/MER catalyst yielded a much lower maximum H₂ production (0.6 μmol H₂ min⁻¹ ≈ 0.08 mmol H₂ g COD_{initial}⁻¹). In literature some studies have also reported a higher catalytic activity and H₂ production with PtRe/C than with Pt/C catalysts (Ciftci et al., 2014a, 2014b; King et al., 2010). These works also concluded that H₂ selectivity with PtRe/C catalysts is lower due to consumption in the hydrogenation of intermediates from dehydration reactions promoted by the acidity of PtRe alloy. Likewise, a role was also attributed to Re in bimetallic

catalysts in enhancing WGS reaction through a higher rate of CO removal from the catalyst surface.

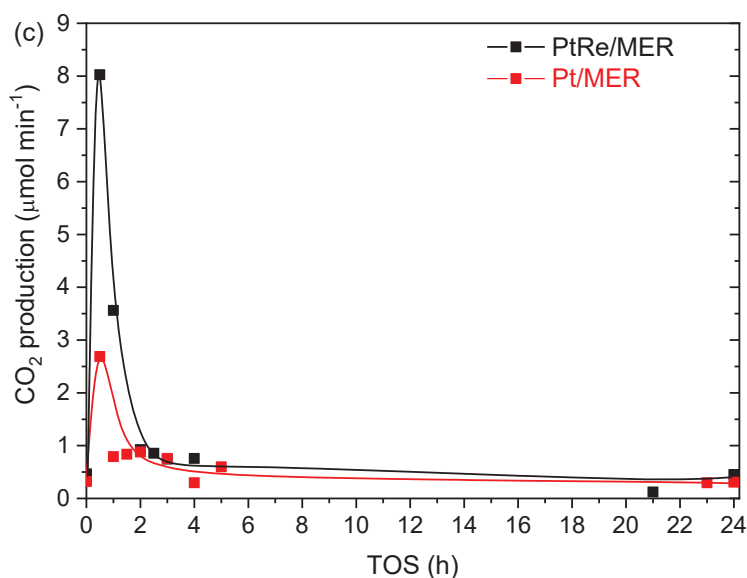
The maximum production of CO₂ occurred also at low TOS. Despite that, it is important to mention that in the current work CO₂ production, and consequently CC gas, are affected by the addition of KOH to brewery wastewater, as KOH reacts with the CO₂ produced giving rise to carbonates in the liquid phase (Oliveira et al., 2020a).

Both Pt/MER and PtRe/MER catalysts showed a similar pattern for the generation of gases, suggesting that both undergo deactivation through a similar mechanism. At long time on stream both catalysts also maintained a similar residual H₂ and CO₂ production. Nevertheless, the H₂ pattern may indicate that deactivation in the case of Pt/MER takes place in the earlier stages, since the maximum of H₂ production was much lower than for PtRe/MER catalyst. Likewise, very low amounts of alkanes were produced throughout the experiment.





245



246

247 Figure 2. (a) H_2 , (b) total alkanes and (c) CO_2 production upon time on stream in the APR
 248 of SBW with Pt/MER and PtRe/MER catalysts (225°C , 28 bar, $\text{WHSV} = 0.12 \text{ h}^{-1}$ and
 249 $V_{\text{Ar}} = 0.4 \text{ cm s}^{-1}$)

250

251 Regarding the composition of the alkanes fraction, CH_4 was by far the major component
 252 (up to 94% of the total alkanes fraction), its percentage decreasing somewhat upon TOS.

253 The decrease was more relevant, from 94 to 81% after 24 h TOS (Figure S3), in the case

of Pt/MER catalyst. Thus, catalyst deactivation affected also CH₄ formation, probably due to reduction of methanation reaction and/or formation of CH₄ precursor intermediates, such as methanol (Shabaker et al., 2003) or acetaldehyde (Godina et al., 2015).

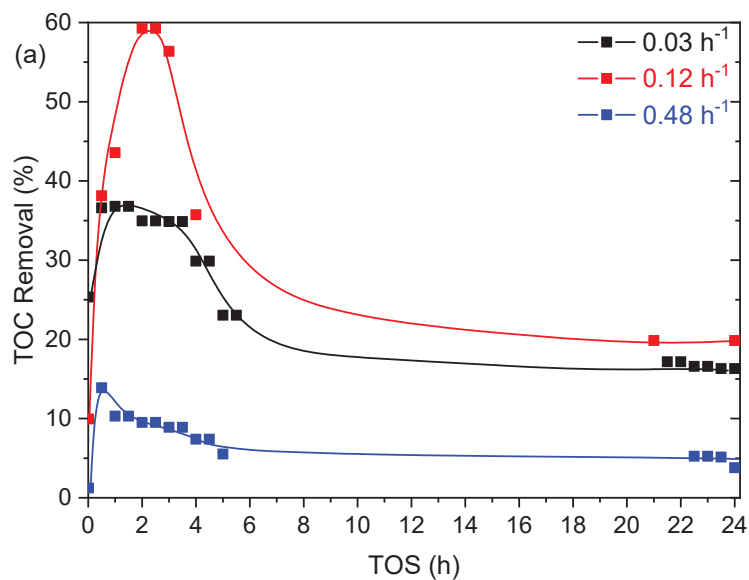
3.2.2. Effect of weight hourly space velocity

In order to investigate the effect of space velocity on the catalytic performance, the brewery wastewater was fed into the reactor at different flow rates, from 0.25 to 4 mL min⁻¹, corresponding to WHSV values from 0.03 to 0.48 h⁻¹. The experiments were performed with the PtRe/MER catalyst, given its higher activity and H₂ production, at a V_{Ar} of 0.4 cm s⁻¹. Figure 3 (a) and (b) shows the evolution of TOC and COD removal upon time on stream. TOC and COD removal was lower as WHSV increased, due to shorter contact time, but no monotonical trend was observed. The removal peak values were achieved for TOS between 1 and 5 h, then followed by a sharp decrease due to deactivation of the catalysts, although some residual activity was maintained.

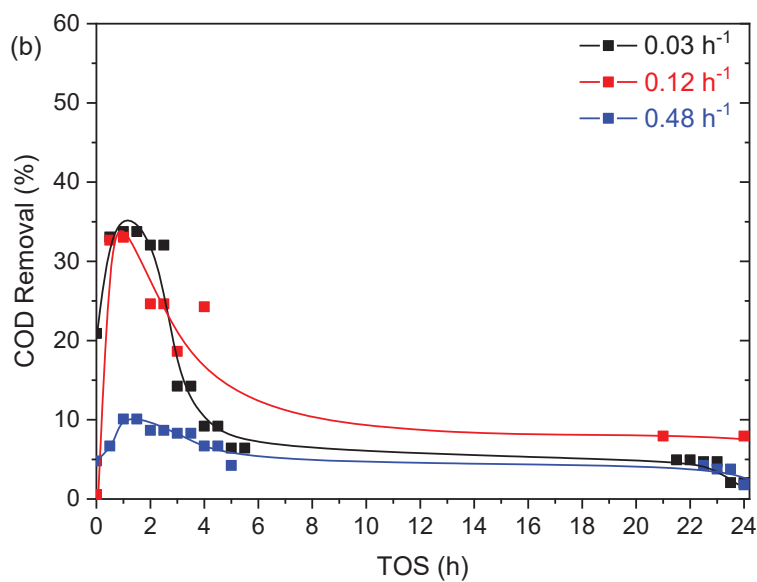
WHSV showed an important influence in the generation of gas products, as can be seen from the results in Figure 3 (c). A clear decrease of CC gas at increasing WHSV took place, associated to lower contact times. Kirilin et al. (2014) and Kim et al. (2012) reported a similar behaviour in the APR of xylitol and ethylene glycol using PtRe catalysts. A sharp decrease of CC gas was observed with TOS, consistent with TOC and COD removal, especially at lower WHSV. After approximately 1 h on stream a remarkable maximum of CC gas of (32.8%) was obtained at the lowest WHSV tested (0.03 h⁻¹), which matches with TOC removal and indicates that the degradation routes leading to gases are favoured by a higher contact between the organic species and the catalyst. When WHSV increased, the peak values of CC gas were lower. This trend is coherent with the lower TOC removal at 0.48 h⁻¹, but, as noted in the previous experiments, the lack of carbon balance closure suggests formation of carbonaceous

279 deposits, most probably upon HTC and deposition of condensation species. The carbon
 280 balance closure in these experiments varied from 41 to 99%.

281



282



283

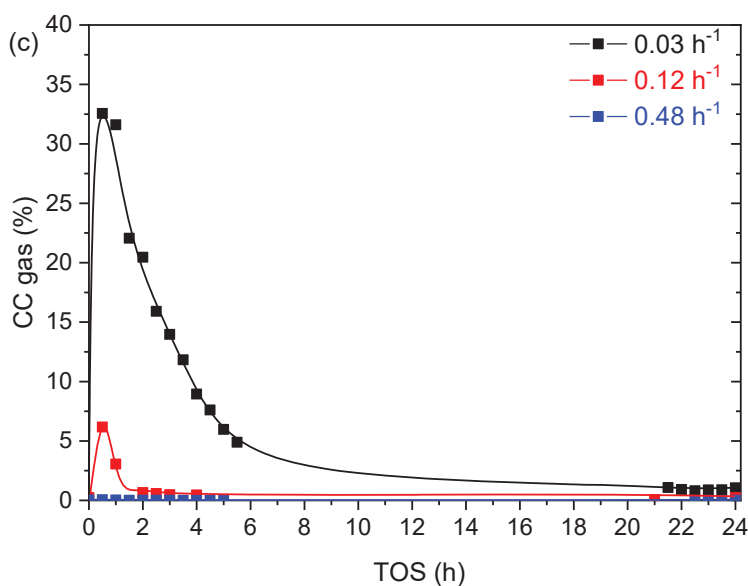
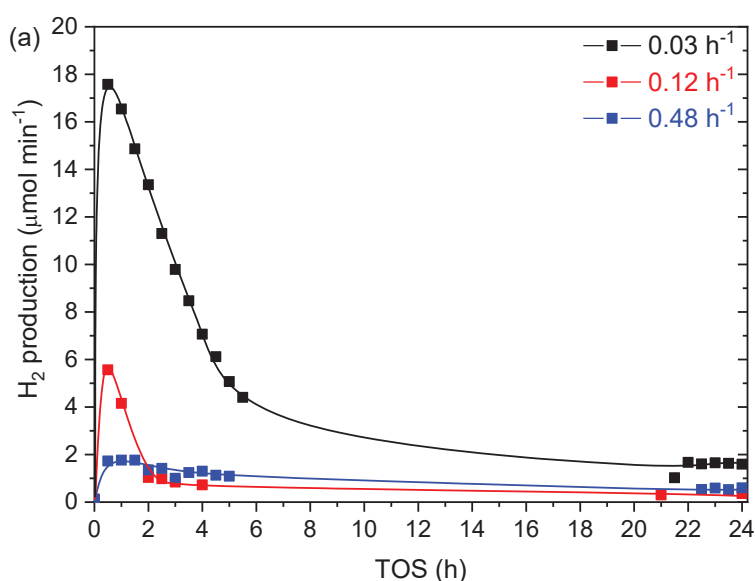


Figure 3. (a) TOC removal, (b) COD removal and (c) CC gas upon time on stream at different WHSV in the APR of SBW with PtRe/MER catalyst (225 °C, 28 bar and $V_{Ar} = 0.4 \text{ cm s}^{-1}$)

Figure 4 represents the production of H_2 , alkanes and CO_2 upon time on stream at different WHSV. All the gas components followed similar trends, reaching a maximum production at low TOS and then decreasing sharply. The peak values for gas production are observed at TOS values shorter than those for TOC and COD removal peak. Likewise, the decline is faster than for TOC and COD removal. At the lowest WHSV (0.03 h^{-1}) the maximum of H_2 production was $17.6 \mu\text{mol min}^{-1}$ (corresponding to $12.5 \text{ mmol H}_2 \text{ g COD}_{\text{initial}}^{-1}$) while the production of alkanes (94.5% of CH_4) and CO_2 was 4.2 and $7.1 \mu\text{mol min}^{-1}$, respectively. The maximum of production of gases significantly decreased when WHSV increased. These results are similar to those reported by Kirilin et al. (2012) in the APR of xylitol under similar conditions (225 °C, 29 bar) using Pt catalyst. They reported that the rate of H_2 formation decreased from around $7 \times 10^{-4} \text{ mol min}^{-1}$ to $6 \times 10^{-4} \text{ mol min}^{-1}$ and the total alkanes formation decreased from $6 \times 10^{-5} \text{ mol min}^{-1}$ to $5 \times 10^{-6} \text{ mol min}^{-1}$.

min⁻¹, while the xylitol conversion decreased from around 65 to 40%, when the WHSV increased from 1.8 to 3.9 h⁻¹. An increase in WHSV implies a higher mass of carbon substrate reacting per time and per mass of catalysts, which could lead to a higher H₂ production as more substrate is available, however, the TOC conversion decreased due to a shorter contact time. Therefore, in the range studied, H₂ production was favoured by low WHSV because of the longer contact time between the catalyst and the organic matter present in the wastewater. However, the H₂ produced also participates in the side reactions for alkanes formation, which justifies a higher alkanes production at lower values of WHSV.

The effect of WHSV on the deactivation of the catalysts is highly significant. At WHSV values of 0.12 and 0.48 h⁻¹ the decrease in the production of H₂ is very fast, whereas it is slower for 0.03 h⁻¹. Again, the catalyst lost almost totally the ability to produce alkanes but maintained a residual production of H₂, which was relatively high (1.8 μmol min⁻¹) at 0.03 h⁻¹.



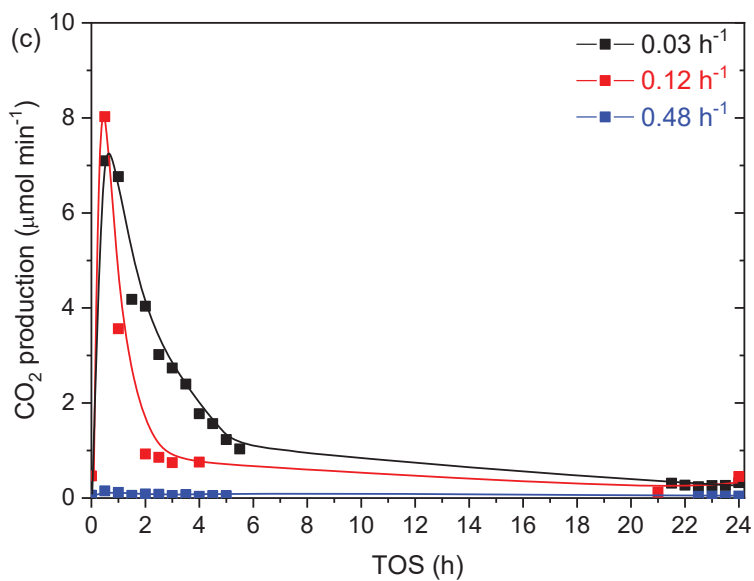
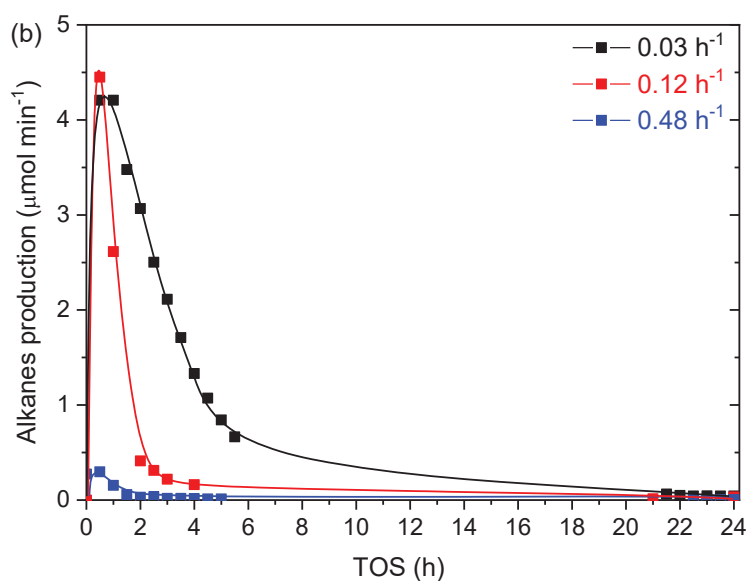
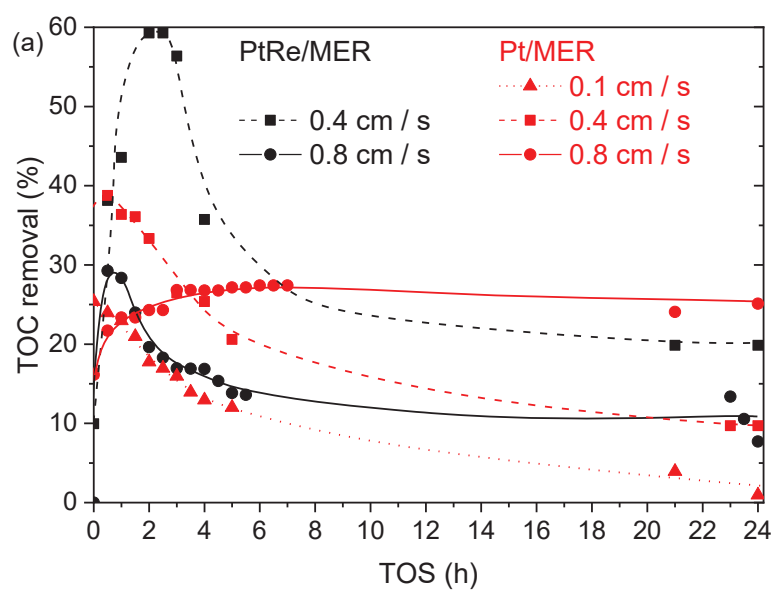


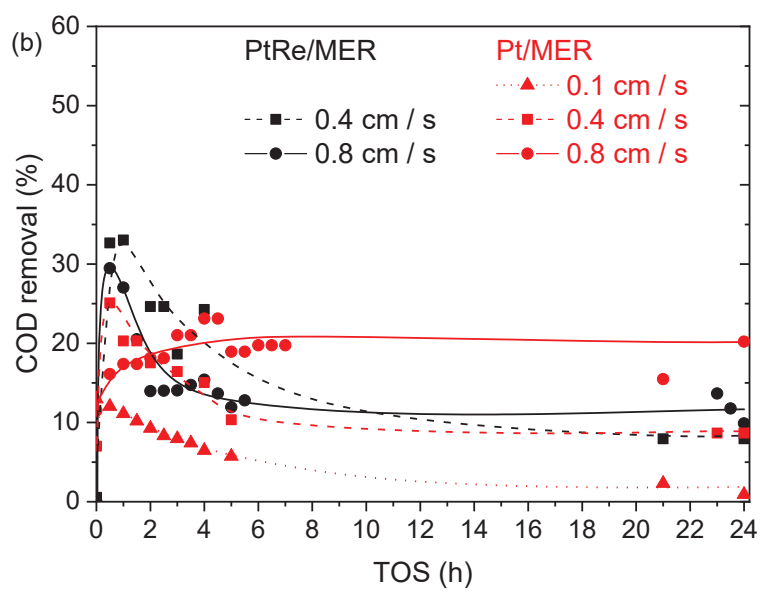
Figure 4. (a) H₂, (b) total alkanes and (c) CO₂ production upon time on stream at different WHSV in the APR of SBW with PtRe/MER catalyst (225 °C, 28 bar and V_{Ar} = 0.4 cm s⁻¹)

3.2.3. Effect of superficial Ar flow velocity

In the current work different V_{Ar} values (0.1, 0.4 and 0.8 cm s⁻¹) were tested, by feeding 5, 20 and 40 N mL min⁻¹ of carrier gas into the reactor. The experiments were performed with Pt/MER and PtRe/MER catalysts at constant intermediate space velocity of 0.12 h⁻¹. Figure 5 shows the effect of V_{Ar} on TOC and COD removal with both catalysts. TOC and COD removal was initially higher at low V_{Ar} (0.1 and 0.4 cm s⁻¹) for both catalysts, but a gradual decline was observed upon time on stream. In the case of Pt/MER, the asymptotic decay of TOC removal suggests that the catalyst finally undergoes nearly complete deactivation. When superficial velocity was increased to 0.8 cm s⁻¹ the initial TOC removal was moderate for Pt/MER in the short-term, but both TOC and COD removal remained quite stable, at around 25 and 19% respectively, during 24 h on stream, evidencing a much better performance and less deactivation of this catalyst at high V_{Ar} . For PtRe/MER catalyst, TOC removal significantly decreased at increasing V_{Ar} . As in the rest of the experiments commented before, CC gas showed a significant decline upon time on stream associated to catalyst deactivation (Figure 5 (c)). CC gas values were higher at higher V_{Ar} with PtRe/MER because of faster removal of the gas products from the catalyst surface. In contrast, a lower TOC removal was observed for this catalyst, probably due to poorer wetting leading to a lower contact between the substrate in the liquid phase and the catalyst (Neira D'Angelo et al., 2013a), although the substrate converted is transformed into gases in a higher extent. In the case of Pt/MER, CC gas was low throughout the experiments (< 2%) and a similar trend was observed for TOC removal (Figure 5 (a)). The carbon balance closure in the experiments with PtRe/MER ranged from 41 to 100%, while in the experiments with Pt/MER the range was from 63 to 99%.



348



349

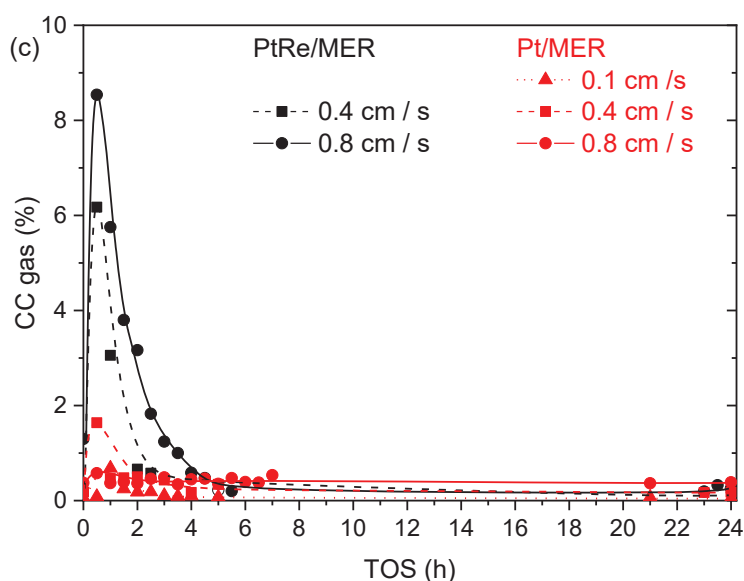


Figure 5. (a) TOC removal, (b) COD removal and (c) CC gas upon time on stream at different V_{Ar} in the APR of SBW with Pt/MER and PtRe/MER catalysts (225 °C, 28 bar and WHSV = 0.12 h⁻¹)

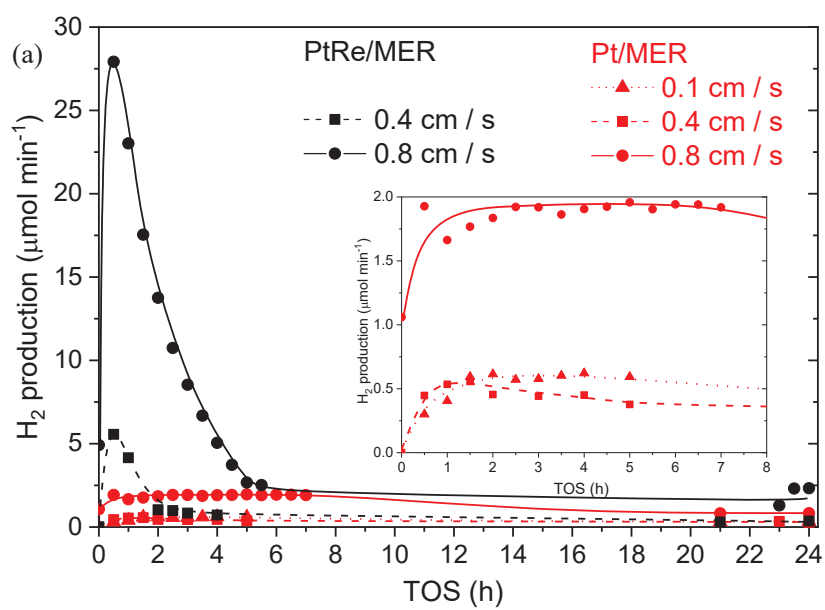
Figure 6 shows the evolution of individual gas components production upon TOS using different V_{Ar} values. Increasing this variable was especially beneficial for H₂ production (Figure 6 (a)). In the case of PtRe/MER, the maximum H₂ production increased from 5.6 to 27.9 $\mu\text{mol min}^{-1}$ (corresponding to 4.2 mmol H₂ g COD_{initial}⁻¹) when V_{Ar} increased from 0.4 to 0.8 cm s⁻¹. For Pt/MER, the maximum H₂ production increased from around 0.5 (V_{Ar} of 0.1 – 0.4 cm s⁻¹) to 1.9 $\mu\text{mol min}^{-1}$ at V_{Ar} of 0.8 cm s⁻¹ (corresponding to 0.3 mmol H₂ g COD_{initial}⁻¹), and interestingly, for this catalyst the maximum H₂ production was maintained for more than 7 h on stream (see zoomed insert in the Figure 6 (a)). This boost in H₂ production can be related to lower consumption in secondary reactions and to shift in reactions leading to H₂ (Neira D'Angelo et al., 2014, 2013b). Neira D'Angelo et al. (2013b) also reported that stripping with N₂ in the APR of sorbitol decreased the partial

pressure of H₂, thus enhancing the reforming reaction rate at the expense of H₂-consuming secondary reactions.

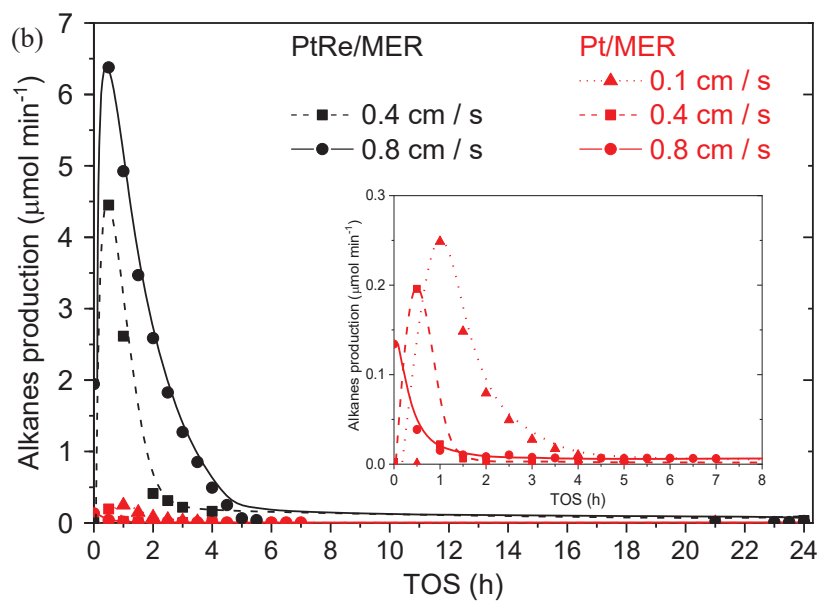
In the case of Pt/MER catalyst, the decrease of alkanes production at increasing V_{Ar} may be related to a lower H₂ availability for secondary reactions (see zoomed insert in the Figure 6 (b)). A sharp decline occurred within a short time on stream. It has to be noted that the maximum alkanes production occurs during the stabilization stage, where H₂ production also increased gradually. H₂ production PtRe/MER decreased after 6 h on stream by more than 92%, compared to peak value, regardless V_{Ar}. The residual H₂ production was higher for a superficial velocity of 0.8 cm s⁻¹, which cannot be only explained in terms of consumption in secondary reactions since the production of alkanes was similar at the two V_{Ar} tested. In fact, the residual production of alkanes was slightly lower at a V_{Ar} of 0.8 cm s⁻¹. However, at low TOS, before deactivation of the catalyst, the generation of alkanes was lower at the lowest V_{Ar} tested.

Respect to CO₂ production, a clear trend could not be observed with V_{Ar}. The maximum production was similar (7.4 – 8.0 μmol min⁻¹) for both V_{Ar} tested with PtRe/MER, while for Pt/MER it was more stable at the highest V_{Ar}.

Finally, the results indicate that there could be an alternative route for H₂ production, independent of catalyst activity under these reaction conditions, since at the highest TOS tested the catalyst can be assumed to be almost completely deactivated but a residual H₂ production is maintained. This route could be related to HTC of the organic matter present in the wastewater. The temperature gradient across the liquid boundary layer in the internal wall of the reactor can contribute to this route, since the temperature was controlled with a thermocouple inserted in the catalytic bed.



390



391

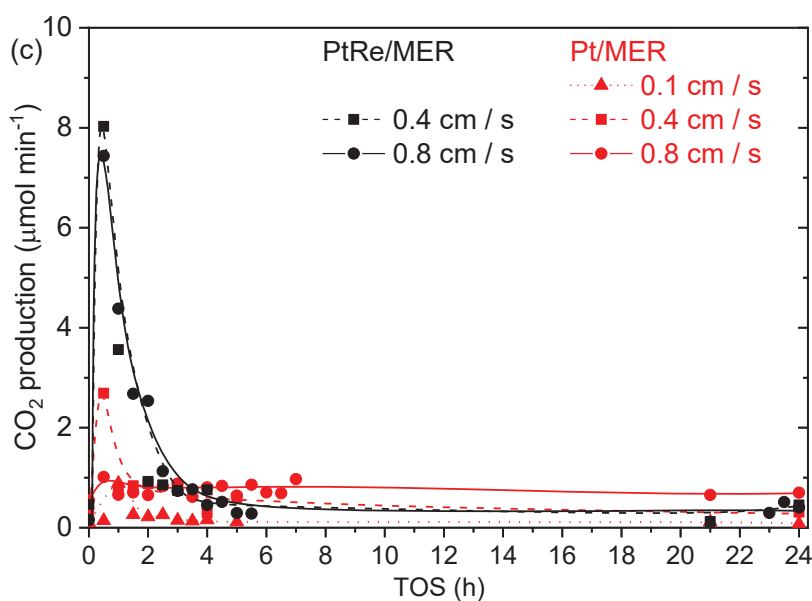


Figure 6. (a) H₂, (b) total alkanes and (c) CO₂ production upon time on stream at different V_{Ar} in the APR of SBW with Pt/MER and PtRe/MER catalysts (225 °C, 28 bar and WHSV = 0.12 h⁻¹)

3.3. Biohydrogen production

Table 1 compares H₂ production performance in the current study and in other recent studies dealing with H₂ production from brewery wastewater. In the current study the maximum H₂ production (27.9 μmol min⁻¹, corresponding to 4.2 mmol H₂ g COD_{initial}⁻¹) was obtained in the first hours of reaction using the PtRe/MER catalyst and the highest V_{Ar} tested (0.8 cm s⁻¹). As can be seen, this value is relatively lower than those previously reported for the APR process in batch experiments, which indicate that H₂ production can be optimized, mainly by overcoming deactivation. However, it is important to highlight that the different reaction conditions between batch and continuous reactors affect the APR process, making difficult a direct comparison of the results.

On the other hand, the maximum H₂ production obtained in previous works for batch APR process were significantly higher than those reported for other technologies, except

for photofermentation with a pretreatment stage (Al-Mohammedawi and Znad, 2020). Nevertheless, in that case the maximum H₂ production was obtained using a mixture of brewery wastewater (30%) and restaurant wastewater, and H₂ production was significantly lower when concentration was increased. Finally, the maximum H₂ production obtained in the current study is among the highest reported, which indicates the potential of the APR process for the treatment and valorisation of wastewater, including brewery wastewater. The highest H₂ production was reported for microbial electrochemical technology (Asensio et al., 2021), showing the potential of this technique if some drawbacks, such as long hydraulic retention and stabilization time, are overcome.

Table 1. The comparison of H₂ production performance of this study with other studies applying different wastewater treatment process

Wastewater treatment process	Operation mode	Feedstock	COD _{initial}	Maximum H ₂ production	Reference
Microbial electrochemical technology - microbial electrochemical fluidized bed reactor	Continuous	RBW	27200 – 51200 mg COD L ⁻¹ d ⁻¹	360 μmol min ⁻¹ *	(Asensio et al., 2021)
Anaerobic treatment - anaerobic fluidized bed reactor	Continuous	RBW	27200 – 51200 mg COD L ⁻¹ d ⁻¹	2.4 μmol min ⁻¹ *	(Asensio et al., 2021)
Pre-treatment stage of biosorbent – sonication + Photofermentation	Batch	Mixture of RBW and restaurant wastewater	3944 mg COD L ⁻¹	12.7 mmol H ₂ g COD _{initial} ⁻¹ *	(Znad et al., 2021)
APR	Batch	RBW and SBW	4764 – 5846 mg COD L ⁻¹	12.9 mmol H ₂ g COD _{initial} ⁻¹	(Oliveira et al., 2020a)
Pretreatment stage + Photofermentation	Batch	Mixture of RBW and restaurant wastewater	2350 – 3290 mg COD L ⁻¹	22.2 mmol H ₂ g COD _{initial} ⁻¹ *	(Al-Mohammedawi and Znad, 2020)
Anaerobic treatment - anaerobic	Batch	RBW and SBW	2500 – 1000 mg COD L ⁻¹	2.0 mmol H ₂ g COD _{initial} ⁻¹ *	(Arantes et al., 2020)

sequencing batch biofilm reactor					
Encapsulated biomass system	Continuous	RBW	3000 – 12000 mg COD L ⁻¹	10 µmol min ⁻¹ *	(Zhu et al., 2019)
APR	Batch	SBW	1531 – 11204 mg COD L ⁻¹	15.4 mmol H ₂ g COD initial ⁻¹	(Oliveira et al., 2019)
Pretreatment stage + Photofermentation	Batch	RBW	2350 – 2837 mg COD L ⁻¹	6.4 mmol H ₂ g COD initial ⁻¹ *	(Al- Mohamme dawi et al., 2019)
APR	Continuous	SBW	6229 mg COD L ⁻¹	27.9 µmol min ⁻¹	Current study

*Estimated from data available

3.4. Catalysts deactivation

The catalysts used were characterized by N₂ adsorption/desorption isotherms, STEM, elemental analysis and TG-TPD/TPO. The textural characteristics and the mean NPs size of the fresh and used catalysts, the elemental analysis, the N₂ adsorption/desorption isotherms and the STEM images and the corresponding histograms representing NPs size distributions are included as supplementary information (Table S2, Table S3, Figure S4 and Figure S5, respectively). After 24 h on stream, all catalysts lost almost all their S_{BET} and microporosity and more than 50% of their mesoporosity, except in the case of the PtRe/MER catalyst when tested at WHSV of 0.03 h⁻¹, which retained about 30% of its initial S_{BET} and part of its micro and mesopore volume. The lower loss of porosity for this last experiment could be attributed to a lower mass of substrate reacting per time and per mass of catalyst at the lowest WHSV (0.03 h⁻¹). The results indicate that all catalysts lost S_{BET} probably due to adsorption of organic species, deposition of condensation species and/or formation of carbonaceous solids on the catalysts surface, which could be a main cause of the observed deactivation.

STEM images of some used catalysts were analysed to investigate the stability of the metal phases. The mean NPs size of Pt/MER catalyst increased moderately ($\approx 20 - 35\%$) after 24 h on stream, suggesting some metal sintering. However, no significant differences could be observed between Pt/MER catalysts tested using different superficial velocity ($V_{Ar} = 0.4 - 0.8 \text{ cm s}^{-1}$). In the case of PtRe/MER, the used catalyst yielded smaller NPs size than the fresh one. The smaller NPs size of PtRe catalysts indicate a stabilization of Pt against sintering at elevated temperatures by the presence of Re, as previously reported in the literature (Falcone et al., 2015). The STEM results indicate that changes in NPs size are not responsible for the strong deactivation suffered by the catalysts during the APR of brewery wastewater. This result is consistent with literature, since other authors have also excluded sintering as major cause of deactivation of Pt based catalysts in APR (de Vlieger et al., 2012; Godina et al., 2018a).

The percentages of H, N and O increased significantly after 24 h on stream and even a moderate increase of S was observed in some cases, while the percentage of C decreased by up to 7% (Table S3). This trend is consistent with the adsorption of organic matter and/or deposition of coke-like matter and/or char from HTC with relatively low degree of carbonization.

The used Pt/MER catalysts also were subjected to TG-TPD/TPO tests. Figure 7 shows the weight-loss TG-TPD/TPO profiles and the corresponding differential curves (DTG) for the fresh and used Pt/MER catalysts. The quantitative weight loss values are summarized in Table S4. The initial peak in TG-TPD curve (Figure 7 (a)) at around 100 °C can be ascribed to the loss of water adsorbed on the catalysts. Beyond this temperature, the fresh catalyst did not show additional weight loss, indicating a good thermal stability conferred by the own nature of the support. On the opposite, the used catalysts exhibit a significant peak extending from 140 to 430 °C that can be attributed to the loss of coke

precursor species or to reactants/products physically adsorbed on the catalyst surface. The increase in the Ar flow rate during the operation of the reactor displaces the main peak towards higher temperatures from 380 to 430 °C, which can be attributed to higher development of deposited structures or to a stronger physisorption. This would be consistent with a lower availability of H₂ for the hydrogenation of precursors of the deposited species. Indeed, a comparison of the quantitative weight losses of these catalysts reveals that the weight loss was lower as the superficial Ar flow velocity increased (Table S4). The percentage of weight loss at V_{Ar} of 0.1 cm s⁻¹ was 9.4%, being reduced to 8.6% when V_{Ar} of 0.8 cm s⁻¹ was used.

Regarding TG-TPO profiles, (Figure 7 (b)) the peak observed for the fresh Pt/MER catalyst is associated with the carbon support burn off. An early initiation of weight loss in TG-TPO and a shift of the peak in DTG-TPO curves towards lower temperatures and was observed upon increasing V_{Ar}. The displacement of the DTG-TPD profiles is in accordance with the aging of the species, which seems to be favoured at the highest V_{Ar}. Likewise, the burning of species below 450 °C suggests the presence of coke-like matter on the catalyst surface. This coke has a major role in the loss of the catalysts porous texture after 24 h on stream (Table S2). Therefore, the formation of solids deposits on the catalyst surface must be a main cause of the strong and early deactivation observed in the APR of brewery wastewater under the reaction conditions tested, particularly when high V_{Ar} is used.

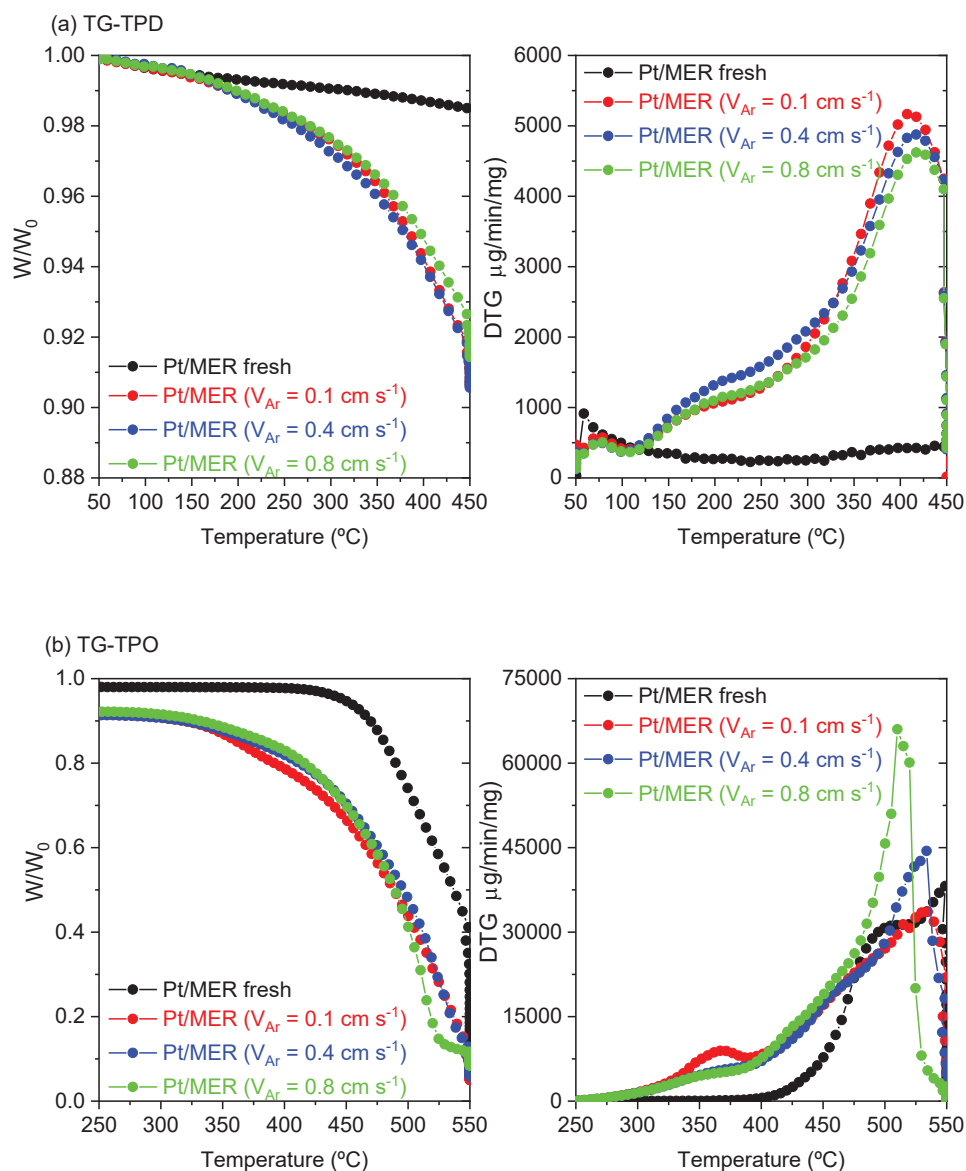


Figure 7. (a) TG-TPD and (b) TG-TPO profiles and the corresponding derivative of fresh and used Pt/MER catalysts

Due to the APR temperature (225 °C), this coke-like carbon material and/or carbon from HTC deposited on the catalyst surface could have been formed from adsorption of the feedstock compounds and/or intermediates formed by side reactions on the metal sites, followed by condensation or polymerization of these precursors, resulting in a film that covers or encapsulates the metal particle (Ochoa et al., 2020). In this sense, relevant precursors of solid humins, such as pyruvaldehyde and HMF, were identified in the APR

of maltose evidencing this formation route (Oliveira et al., 2021). In addition to this, formation of hydrothermal carbon has been observed as relevant competing reaction in previous works on APR of brewery wastewater (Oliveira et al., 2019).

Finally, although the APR process has potential advantages for H₂ production compared to other methods, the deactivation of catalysts, in particular by coking, is a major drawback for the process and may hinder the commercial prospects. Therefore, future efforts must be related to the search for conditions or combined processes that avoid catalyst deactivation and regeneration. The pretreatment of the feedstock by hydrogenation (Oliveira et al., 2021) or oxidation (Oliveira et al., 2020b), for example, could be used as methods to reduce the formation of carbonaceous deposits and improve catalyst stability.

4. Conclusions

Pt/C and PtRe/C catalyst were tested in the continuous APR of a synthetic brewery wastewater for H₂ production. Despite the different reaction conditions tested, a strong catalyst deactivation was observed during the first hours on stream. Before deactivation, PtRe catalyst was more active than Pt one and the maximum of H₂ production increased with decreasing the WHSV (from 0.48 to 0.03 h⁻¹) and increasing the V_{Ar} (from 0.1 to 0.8 cm s⁻¹). The maximum of H₂ production obtained (27.9 μmol min⁻¹) under the different conditions tested was relatively higher than almost all other continuous brewery wastewater treatment process, showing the potential of the process for H₂ production. The catalysts deactivation was attributed to the adsorption of organic matter and/or deposition of solids on the catalysts surface. Therefore, the prospects for the future development of

the process must be related to improvements in the stability of the catalyst and coking minimization.

Acknowledgements

The authors greatly appreciate financial support from Spanish MINECO (CTQ2015-65491-R) and Comunidad de Madrid (BIOTRES-CM P2018/EMT-4344). A. S. Oliveira thanks the Spanish MINECO a research grant (BES-2016-077244).

References

- Aho, A., Rosales, C., Eränen, K., Salmi, T., Murzin, D.Y., Grénman, H., 2020. Biohydrogen from dilute side streams - Influence of reaction conditions on the conversion and selectivity in aqueous phase reforming of xylitol. *Biomass and Bioenergy* 138, 105590. <https://doi.org/10.1016/j.biombioe.2020.105590>
- Al-Mohammedawi, H.H., Znad, H., 2020. Impact of metal ions and EDTA on photofermentative hydrogen production by *Rhodobacter sphaeroides* using a mixture of pre-treated brewery and restaurant effluents. *Biomass and Bioenergy* 134, 105482. <https://doi.org/10.1016/j.biombioe.2020.105482>
- Al-Mohammedawi, H.H., Znad, H., Eroglu, E., 2019. Improvement of photofermentative biohydrogen production using pre-treated brewery wastewater with banana peels waste. *Int. J. Hydrogen Energy* 44, 2560–2568. <https://doi.org/10.1016/j.ijhydene.2018.11.223>

540 Arantes, M.K., Sequinel, R., Alves, H.J., Machado, B., Fiorini, A., da Silva, E.A., 2020.
 541 Improvement of biohydrogen production from brewery wastewater: Evaluation of
 542 inocula, support and reactor. *Int. J. Hydrogen Energy* 45, 5216–5226.
 543 <https://doi.org/10.1016/j.ijhydene.2019.07.208>

544 Asensio, Y., Llorente, M., Fernández, P., Tejedor-Sanz, S., Ortiz, J.M., Ciriza, J.F.,
 545 Monsalvo, V., Rogalla, F., Esteve-Núñez, A., 2021. Upgrading fluidized bed
 546 bioelectrochemical reactors for treating brewery wastewater by using a fluid-like
 547 electrode. *Chem. Eng. J.* 406, 127103. <https://doi.org/10.1016/j.cej.2020.127103>

548 Chia, M., J. Pagán-Torres, Y., Hibbitts, D., Tan, Q., N. Pham, H., K. Datye, A., Neurock,
 549 M., J. Davis, R., A. Dumesic, J., 2011. Selective hydrogenolysis of polyols and
 550 cyclic ethers over bifunctional surface sites on rhodium–rhenium catalysts. *J. Am.*
 551 *Chem. Soc.* 133, 12675–12689. <https://doi.org/10.1021/ja2038358>

552 Ciftci, A., Ligthart, D.A.J.M., Hensen, E.J.M., 2014a. Aqueous phase reforming of
 553 glycerol over Re-promoted Pt and Rh catalysts. *Green Chem.* 16, 853–863.
 554 <https://doi.org/10.1039/C3GC42046A>

555 Ciftci, A., Ligthart, D.A.J.M., Sen, A.O., Van Hoof, A.J.F., Friedrich, H., Hensen, E.J.M.,
 556 2014b. Pt-Re synergy in aqueous-phase reforming of glycerol and the water-gas shift
 557 reaction. *J. Catal.* 311, 88–101. <https://doi.org/10.1016/j.jcat.2013.11.011>

558 Cortright, R.D., Davda, R.R., Dumesic, J.A., 2002. Hydrogen from catalytic reforming
 559 of biomass-derived hydrocarbons in liquid water. *Nature* 418, 964–967.
 560 <https://doi.org/10.1038/nature01009>

561 Davda, R.R., Shabaker, J.W., Huber, G.W., Cortright, R.D., Dumesic, J.A., 2005. A
 562 review of catalytic issues and process conditions for renewable hydrogen and
 563 alkanes by aqueous-phase reforming of oxygenated hydrocarbons over supported

564 metal catalysts. *Appl. Catal. B Environ.* 56, 171–186.
 565 <https://doi.org/10.1016/j.apcatb.2004.04.027>

566 Davda, R.R., Shabaker, J.W., Huber, G.W., Cortright, R.D., Dumesic, J.A., 2003.
 567 Aqueous-phase reforming of ethylene glycol on silica-supported metal catalysts.
 568 *Appl. Catal. B Environ.* 43, 13–26. [https://doi.org/10.1016/S0926-3373\(02\)00277-1](https://doi.org/10.1016/S0926-3373(02)00277-1)

569 de Vlieger, D.J.M., Thakur, D.B., Lefferts, L., Seshan, K., 2012. Carbon Nanotubes: A
 570 Promising Catalyst Support Material for Supercritical Water Gasification of
 571 Biomass Waste. *ChemCatChem* 4, 2068–2074.
 572 <https://doi.org/10.1002/cctc.201200318>

573 Duarte, H.A., Sad, M.E., Apesteguía, C.R., 2017. Production of bio-hydrogen by liquid
 574 processing of xylitol on Pt/Al₂O₃ catalysts: Effect of the metal loading. *Int. J.*
 575 *Hydrogen Energy* 42, 4051–4060.
 576 <https://doi.org/10.1016/J.IJHYDENE.2016.11.119>

577 Godina, L.I., Kirilin, A. V., Tokarev, A. V., Murzin, D.Y., 2015. Aqueous phase
 578 reforming of industrially relevant sugar alcohols with different chiralities. *ACS*
 579 *Catal.* 5, 2989–3005. <https://doi.org/10.1021/cs501894e>

580 Godina, L.I., Kirilin, A. V., Tokarev, A. V., Simakova, I.L., Murzin, D.Y., 2018a.
 581 Sibunit-supported mono- and bimetallic catalysts used in aqueous-phase reforming
 582 of xylitol. *Ind. Eng. Chem. Res.* 57, 2050–2067.
 583 <https://doi.org/10.1021/acs.iecr.7b04937>

584 Godina, L.I., Tokarev, A. V., Simakova, I.L., Mäki-Arvela, P., Kortesmäki, E., Gläsel, J.,
 585 Kronberg, L., Etzold, B., Murzin, D.Y., 2018b. Aqueous-phase reforming of
 586 alcohols with three carbon atoms on carbon-supported Pt. *Catal. Today* 301, 78–89.
 587 <https://doi.org/10.1016/j.cattod.2017.03.042>

588 Habte Lemji, H., Eckstädt, H., 2013. A pilot scale trickling filter with pebble gravel as
 589 media and its performance to remove chemical oxygen demand from synthetic
 590 brewery wastewater. *J. Zhejiang Univ. B (Biomedicine Biotechnol.* 14, 924–933.
 591 <https://doi.org/10.1631/jzus.B1300057>

592 Huber, G.W., Shabaker, J.W., Evans, S.T., Dumesic, J.A., 2006. Aqueous-phase
 593 reforming of ethylene glycol over supported Pt and Pd bimetallic catalysts. *Appl.*
 594 *Catal. B Environ.* 62, 226–235. <https://doi.org/10.1016/j.apcatb.2005.07.010>

595 Khodabandehloo, M., Larimi, A., Khorasheh, F., 2020. Comparative process modeling
 596 and techno-economic evaluation of renewable hydrogen production by glycerol
 597 reforming in aqueous and gaseous phases. *Energy Convers. Manag.* 225, 113483.
 598 <https://doi.org/10.1016/j.enconman.2020.113483>

599 Kim, H.D., Park, H.J., Kim, T.W., Jeong, K.E., Chae, H.J., Jeong, S.Y., Lee, C.H., Kim,
 600 C.U., 2012. The effect of support and reaction conditions on aqueous phase
 601 reforming of polyol over supported Pt-Re bimetallic catalysts. *Catal. Today* 185, 73–
 602 80. <https://doi.org/10.1016/j.cattod.2011.08.012>

603 King, D.L., Zhang, L., Xia, G., Karim, A.M., Heldebrant, D.J., Wang, X., Peterson, T.,
 604 Wang, Y., 2010. Aqueous phase reforming of glycerol for hydrogen production over
 605 Pt-Re supported on carbon. *Appl. Catal. B Environ.* 99, 206–213.
 606 <https://doi.org/10.1016/j.apcatb.2010.06.021>

607 Kirilin, A. V., Tokarev, A. V., Kustov, L.M., Salmi, T., Mikkola, J.-P., Murzin, D.Y.,
 608 2012. Aqueous phase reforming of xylitol and sorbitol: Comparison and influence
 609 of substrate structure. *Appl. Catal. A Gen.* 435–436, 172–180.
 610 <https://doi.org/10.1016/j.apcata.2012.05.050>

611 Kirilin, A. V., Tokarev, A. V., Manyar, H., Hardacre, C., Salmi, T., Mikkola, J.-P.,

612 Murzin, D.Y., 2014. Aqueous phase reforming of xylitol over Pt-Re bimetallic
 613 catalyst: Effect of the Re addition. *Catal. Today* 223, 97–107.
 614 <https://doi.org/10.1016/j.cattod.2013.09.020>

615 Martín, M., Grossmann, I.E., 2014. Optimal simultaneous production of hydrogen and
 616 liquid fuels from glycerol: Integrating the use of biodiesel byproducts. *Ind. Eng.*
 617 *Chem. Res.* 53, 7730–7745. <https://doi.org/10.1021/ie500067d>

618 Neira D'Angelo, M.F., Ordonsky, V., Paunovic, V., Van Der Schaaf, J., Schouten, J.C.,
 619 Nijhuis, T.A., 2013a. Hydrogen production through aqueous-phase reforming of
 620 ethylene glycol in a washcoated microchannel. *ChemSusChem* 6, 1708–1716.
 621 <https://doi.org/10.1002/cssc.201200974>

622 Neira D'Angelo, M.F., Ordonsky, V., van der Schaaf, J., Schouten, J.C., Nijhuis, T.A.,
 623 2013b. Aqueous phase reforming in a microchannel reactor: the effect of mass
 624 transfer on hydrogen selectivity. *Catal. Sci. Technol.* 3, 2834–2842.
 625 <https://doi.org/10.1039/c3cy00577a>

626 Neira D'Angelo, M.F., Ordonsky, V., Van Der Schaaf, J., Schouten, J.C., Nijhuis, T.A.,
 627 2014. Continuous hydrogen stripping during aqueous phase reforming of sorbitol in
 628 a washcoated microchannel reactor with a Pt-Ru bimetallic catalyst. *Int. J. Hydrogen*
 629 *Energy* 39, 18069–18076. <https://doi.org/10.1016/j.ijhydene.2014.02.167>

630 Ochoa, A., Bilbao, J., Gayubo, A.G., Castaño, P., 2020. Coke formation and deactivation
 631 during catalytic reforming of biomass and waste pyrolysis products: A review.
 632 *Renew. Sustain. Energy Rev.* 119, 109600.
 633 <https://doi.org/10.1016/j.rser.2019.109600>

634 Oliveira, A.S., Baeza, J.A., Calvo, L., Alonso-Morales, N., Heras, F., Lemus, J.,
 635 Rodríguez, J.J., Gilarranz, M.A., 2018. Exploration of the treatment of fish-canning

636 industry effluents by aqueous-phase reforming using Pt/C catalysts. *Environ. Sci.*
637 *Water Res. Technol.* 4, 1979–1987. <https://doi.org/10.1039/c8ew00414e>

638 Oliveira, A.S.S., Aho, A., Baeza, J.A.A., Calvo, L., Simakova, I.L.L., Gilarranz, M.A.A.,
639 Murzin, D.Y., 2021. Enhanced H₂ production in the aqueous-phase reforming of
640 maltose by feedstock pre-hydrogenation. *Appl. Catal. B Environ.* 281, 119469.
641 <https://doi.org/10.1016/j.apcatb.2020.119469>

642 Oliveira, A.S.S., Baeza, J.A.A., Calvo, L., Alonso-Morales, N., Heras, F., Rodriguez,
643 J.J.J., Gilarranz, M.A.A., 2019. Production of hydrogen from brewery wastewater
644 by aqueous phase reforming with Pt/C catalysts. *Appl. Catal. B Environ.* 245, 367–
645 375. <https://doi.org/10.1016/j.apcatb.2018.12.061>

646 Oliveira, A.S.S., Baeza, J.A.A., Garcia, D., Saenz de Miera, B., Calvo, L., Rodriguez,
647 J.J.J., Gilarranz, M.A.A., 2020a. Effect of basicity in the aqueous phase reforming
648 of brewery wastewater for H₂ production. *Renew. Energy* 148, 889–896.
649 <https://doi.org/10.1016/J.RENENE.2019.10.173>

650 Oliveira, A.S.S., Baeza, J.A.A., Saenz de Miera, B., Calvo, L., Rodriguez, J.J.J.,
651 Gilarranz, M.A.A., 2020b. Aqueous phase reforming coupled to catalytic wet air
652 oxidation for the removal and valorisation of phenolic compounds in wastewater. *J.*
653 *Environ. Manage.* 274, 111199. <https://doi.org/10.1016/j.jenvman.2020.111199>

654 Pipitone, G., Zoppi, G., Bocchini, S., Rizzo, A.M., Chiaramonti, D., Pirone, R., Bensaid,
655 S., 2020. Aqueous phase reforming of the residual waters derived from lignin-rich
656 hydrothermal liquefaction: investigation of representative organic compounds and
657 actual biorefinery streams. *Catal. Today* 345, 237–250.
658 <https://doi.org/10.1016/j.cattod.2019.09.040>

659 Saenz de Miera, B., Oliveira, A.S.S., Baeza, J.A.A., Calvo, L., Rodriguez, J.J.J.,

660 Gilarranz, M.A.A., 2020. Treatment and valorisation of fruit juice wastewater by
 661 aqueous phase reforming: Effect of pH, organic load and salinity. *J. Clean. Prod.*
 662 252, 119849. <https://doi.org/10.1016/J.JCLEPRO.2019.119849>

663 Shabaker, J.W., Davda, R.R., Huber, G.W., Cortright, R.D., Dumesic, J.A., 2003.
 664 Aqueous-phase reforming of methanol and ethylene glycol over alumina-supported
 665 platinum catalysts. *J. Catal.* 215, 344–352. [https://doi.org/10.1016/S0021-](https://doi.org/10.1016/S0021-9517(03)00032-0)
 666 9517(03)00032-0

667 Shabaker, J.W., Huber, G.W., Dumesic, J., 2004. Aqueous-phase reforming of
 668 oxygenated hydrocarbons over Sn-modified Ni catalysts. *J. Catal.* 222, 180–191.
 669 <https://doi.org/10.1016/j.jcat.2003.10.022>

670 Sladkovskiy, D.A., Godina, L.I., Semikin, K. V., Sladkovskaya, E. V., Smirnova, D.A.,
 671 Murzin, D.Y., 2018. Process design and techno-economical analysis of hydrogen
 672 production by aqueous phase reforming of sorbitol. *Chem. Eng. Res. Des.* 134, 104–
 673 116. <https://doi.org/10.1016/j.cherd.2018.03.041>

674 Zhang, L., Karim, A.M., Engelhard, M.H., Wei, Z., King, D.L., Wang, Y., 2012.
 675 Correlation of Pt-Re surface properties with reaction pathways for the aqueous-
 676 phase reforming of glycerol. *J. Catal.* 287, 37–43.
 677 <https://doi.org/10.1016/j.jcat.2011.11.015>

678 Zhu, K., Arnold, W.A., Novak, P.J., 2019. Modeling alginate encapsulation system for
 679 biological hydrogen production. *Biotechnol. Bioeng.* 116, 3189–3199.
 680 <https://doi.org/10.1002/bit.27152>

681 Znad, H., Al-Mohammedawi, H., Awual, M.R., 2021. Integrated pre-treatment stage of
 682 biosorbent – sonication for mixed brewery and restaurant effluents to enhance the
 683 photo-fermentative hydrogen production. *Biomass and Bioenergy* 144, 105899.